THE JOURNAL OF PHYSICAL CHEMISTRY Letters

pubs.acs.org/JPCL

Letter

Evidence of Facilitated Transport in Crowded Nanopores

Anh Phan* and Alberto Striolo*

Cite This: *J. Phys. Chem. Lett.* 2020, 11, 1814−1821

Read Online

ACCESS | Metrics & More | Article Recommendations | Supporting Information

ABSTRACT: Fluid transport in nature often occurs through crowded nanopores, where a number of phenomena can affect it, because of fluid−fluid and fluid−solid interactions, as well as the presence of organic compounds filling the pores and their structural fluctuations. Employing molecular dynamics, we probe here the transport of fluid mixtures (CO_2−CH_4 and H_2S−CH_4) through silica nanopores filled with benzene. Both CO_2 and H_2S are strongly adsorbed within the organic-filled pore, partially displacing benzene. Unexpectedly, CO_2/H_2S adsorption facilitates CH_4 transport. Analysis of the trajectories suggests that both CO_2 and H_2S act as vehicle-like carriers and might swell benzene, generating preferential transport pathways within the crowded pore. The results are useful for identifying unexpected transport mechanisms and for developing engineering approaches that could lead to storage of CO_2 in caprocks.

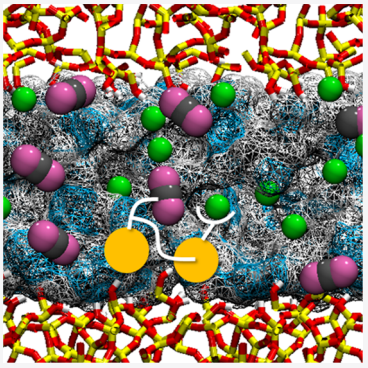

Carbon dioxide (CO_2) injection in geologic reservoirs could provide one solution for carbon capture and storage (CCS).[1−3] Fine-grained sedimentary rocks (shales and mudstone) can provide caprocks in CCS sites.[4,5] These rocks also play important roles in shale gas production.[6] As-produced shale gas from Haynesville and Barnett shales in the United States and Horn River in western Canada contains various amounts of CO_2,[7−11] and up to several hundred parts per million of hydrogen sulfide (H_2S), even in sites in which H_2S was absent in initial assessments.[12] The produced gas is "sweetened"[8,10] to avoid harmful effects on health, safety, and the environment.[13] In some cases, it might be attractive to reinject both H_2S and CO_2 into the formation.[14]

A comprehensive understanding of the fundamental mechanisms responsible for carbon bearing-fluid migration in the presence of CO_2/H_2S is crucial for risk assessment and site selection for geologic CCS, monitoring H_2S emissions, and perhaps identifying innovative enhanced oil recovery (EOR) processes that use CO_2 and H_2S.[15,16] Because a thorough quantification of the phenomena that govern fluid transport in the complex heterogeneous pore networks found in organic-rich shale caprocks, which consist of crowded nanopores that provide poor connections between dispersed pockets of organic matter, remains elusive, because of practical difficulties in observing fluid transport in such complicated systems, computational approaches could be helpful.[17−20]

This study probes transport of systems containing CO_2, H_2S, and methane (CH_4), through a realistic ∼2 nm amorphous silica nanopore saturated with benzene molecules, a model to mimic organic-rich shale caprocks. The number of benzene molecules introduced in the system (400) was sufficient to fill the pore volume and form thin layers on the solid substrate outside the pore (see Figure S1 of the Supporting Information, panel A). The transport results are complemented by careful analysis of mutual solubility, free-energy profiles, and structure of the confined systems. Atomistic molecular dynamics (MD) simulations are conducted at geological temperature (300 K) and pressure (∼13.9 MPa) conditions.[21,22] Various system compositions in the bulk reservoirs are considered, as shown in Figure S1, panel B. Once equilibrium was achieved, system properties such as density profiles for CO_2, H_2S, CH_4, and benzene molecules were determined within the pore as well as in the bulk reservoirs (see Table 1). Details regarding simulation models, algorithms, methods, and computational procedures are reported in the Supporting Information.

We calculated the solubility of CO_2, H_2S, and CH_4 in confined benzene as a function of system composition. The results (Figure 1A, left panel) suggest that CO_2 and H_2S solubility increase linearly when the respective bulk mole fractions increase to 0.21 and 0.12. H_2S (yellow) is more soluble in confined benzene than CO_2 (blue), achieving a solubility coefficient of 7.26 (0.33 MPa^{-1}) compared to 2.38 (0.13 MPa^{-1}) for CO_2. For comparison, H_2S is more soluble in bulk benzene than CO_2, with experimental solubility coefficients being 0.56 MPa^{-1} for H_2S and 0.15 MPa^{-1} for CO_2 at ∼300 K.[23,24] Because bulk simulations overestimate the experimental solubility, the results in Figure 1A suggest that confinement strongly reduces the solubility of H_2S and CO_2 in benzene, which is contrary to many results for other confined systems, in which confinement increases solubility.[25,26] It is possible that

Received: December 17, 2019
Accepted: January 24, 2020
Published: January 24, 2020

https://dx.doi.org/10.1021/acs.jpclett.9b03751
J. Phys. Chem. Lett. 2020, 11, 1814−1821

Table 1. Mole Fraction of CH_4, CO_2, and H_2S in the Bulk Reservoirs as Well as Number of CH_4, CO_2, H_2S, and Benzene Molecules Confined in the Pore for All Systems Simulated after Equilibration Was Achieved

	bulk reservoirs		pore		
system	x_{CO_2}	x_{CH_4}	n_{CO_2}	n_{CH_4}	$n_{C_6H_6}$
0	0.0	1.0	0	97	236
1C	0.03	0.97	13	98	231
2C	0.05	0.95	28	96	227
3C	0.10	0.90	51	88	220
4C	0.21	0.79	102	77	204
5C	0.27	0.73	122	78	192
6C	0.30	0.70	151	72	184
7C	0.34	0.66	167	71	176
8C	0.40	0.60	183	64	175
	x_{H_2S}	x_{CH_4}	n_{H_2S}	n_{CH_4}	$n_{C_6H_6}$
1H	0.02	0.98	21	100	227
2H	0.03	0.97	43	95	221
3H	0.06	0.94	80	89	208
4H	0.12	0.88	152	83	180
5H	0.15	0.85	170	84	172
6H	0.19	0.81	196	80	160
7H	0.21	0.79	220	79	152

confined benzene cannot solvate CO_2 and H_2S molecules as effectively as it does in the bulk, a mechanism similar to the one invoked to explain the lower H_2S solubility in confined water.[27]

Our results show that loading H_2S into the benzene-filled SiO_2 pore enhances the solubility of CH_4 in the same pore, while adding CO_2 reduces CH_4 solubility (Figure 1A, right panel). This observation could have ramifications for improving shale gas extraction. Our simulations also suggest that CH_4 is less strongly adsorbed in the SiO_2 pore filled with benzene compared to H_2S and CO_2 (see Figure S2).

The amount of benzene confined in the nanopore decreases as the bulk mole faction of CO_2 (blue) and H_2S (yellow) increases (Figure 1B). In particular, our analysis suggests that 10 H_2S molecules displace 4 C_6H_6 molecules from the pore, while 10 CO_2 molecules displace 3 C_6H_6 molecules (see Figure S3). These results suggest that varying the minority fluids mixed with CH_4 strongly affects the structure of organics trapped in caprock nanopores and might also be responsible for the pronounced differences observed for CH_4 solubility in confined benzene (Figure 1A, right panel).

To assess whether the results shown in Figure 1A,B are representative of equilibrated systems, we carried out adsorption−desorption cycles. By employing the "evaporate" and "deposit" procedures available in the software package,[28] we extracted CO_2/H_2S molecules and simultaneously inserted CH_4 molecules into the simulated systems. The results in Figure 1A,B show negligible adsorption−desorption hysteresis, suggesting that all simulated processes are reversible and that the results represent equilibrated systems. The results show (Figure 1B) that reducing the bulk CO_2/H_2S mole fraction prompts benzene readsorption into the SiO_2 nanopore.

To document the molecular structure of benzene inside the crowded pore, we calculated in-plane surface density distributions of benzene carbon atoms within layers parallel to the pore surfaces. The results for CO_2−CH_4 (left) and H_2S−CH_4 (right) mixtures are shown in Figure 1C. Details regarding the layer positions are presented in Figure S4. The first and fourth layers are near the bottom and top silica surfaces, respectively, while the second and third layers are approximately in the middle of the pore. The high-density areas (red-yellow spots) of the contour plots indicate positions where the benzene molecules preferentially reside. The results strongly suggest that the distributions of benzene molecules in the first and fourth layers are not altered by the presence of CO_2 and H_2S, indicating that the adsorbed CO_2/H_2S molecules are not able to displace the benzene molecules adsorbed on the pore surfaces. Rather, they displace the benzene molecules accumulated in the middle of the pore, with the result that the distribution of corresponding benzene molecules changes significantly as the CO_2/H_2S bulk mole fraction increases. The density profiles suggest that H_2S displaces more benzene than CO_2 does, which is consistent with the results of Figure 1B. We conducted additional simulations for some systems in which the SiO_2 pore was initially exposed to CO_2/H_2S and subsequently to benzene. The results for the distributions of benzene molecules near the silica surfaces were similar to those shown in Figure 1C, which suggests preferential adsorption of benzene on silica for the systems considered here.

To understand the results shown in Figure 1, we calculated the adsorption energy of benzene, CH_4, CO_2, and H_2S in the nanopore filled with benzene and CH_4 (system 0 in Table 1 and Figure S1) using the two-box approach proposed by Heinz.[29] This method involves the simulation of the adsorbate within the pore and in bulk (Figure 2A). The results in Figure 2B show that H_2S is more strongly adsorbed than the other species, achieving an adsorption energy of −2.13 eV. To compare the values in Figure 2, we refer to ab initio studies of H_2S−benzene, CO_2−benzene, CH_4−benzene, and benzene−benzene dimers.[30−33] The corresponding interaction energies are approximately −2.83, −2.55, −1.47, and −1.81 to −2.78 kcal/mol, respectively.[30−33] The results in Figure 2 explain why benzene is displaced more effectively by H_2S than by CO_2. The interaction energies for benzene−benzene dimers with the T-shaped and parallel-displaced configurations are −2.74 and −2.78 kcal/mol,[32] both stronger than that reported for CO_2−benzene dimers (−2.55 kcal/mol);[30] the highly positive adsorption energy calculated here (0.44 eV, see Figure 2B) suggests that benzene is unlikely to be adsorbed in the nanopore considered, probably because the pore is already filled.

A pressure gradient is imposed through the benzene-filled nanopore via implementing boundary driven nonequilibrium simulations (see Figure S5). As a function of the pressure gradient, a molecular flux is established. Once the steady-state flow is achieved, we extracted molar fluxes, permeability, and transport diffusivity (D_t). The latter is quantified in the limit of the external force approaching zero, when the structure of the benzene-filled pore should remain unchanged in response to the applied pressure. This is confirmed via in-plane density distributions at equilibrium and during flow (Figure S6).

In Figure 3A, the permeabilities are shown for CO_2 and H_2S (left panel, blue and yellow, respectively) as well as CH_4 mixed with CO_2/H_2S (right panel, blue/yellow) as a function of system composition. We considered only those systems with CO_2 (/H_2S) mole fraction <0.21 (/0.12) as these exhibit linear changes in the adsorption isotherms (see Figure 1A) and because the CH_4 mole fraction in shale gas is typically >0.8.[34,35] The results in Figure 3A show that H_2S permeates the pore much faster than CO_2 and CH_4. Increasing both CO_2 and H_2S bulk mole fraction enhances the permeability of all species, probably because CO_2 and H_2S displace benzene from the pore, opening preferential pathways across the crowded nanopore.

https://dx.doi.org/10.1021/acs.jpclett.9b03751
J. Phys. Chem. Lett. 2020, 11, 1814−1821

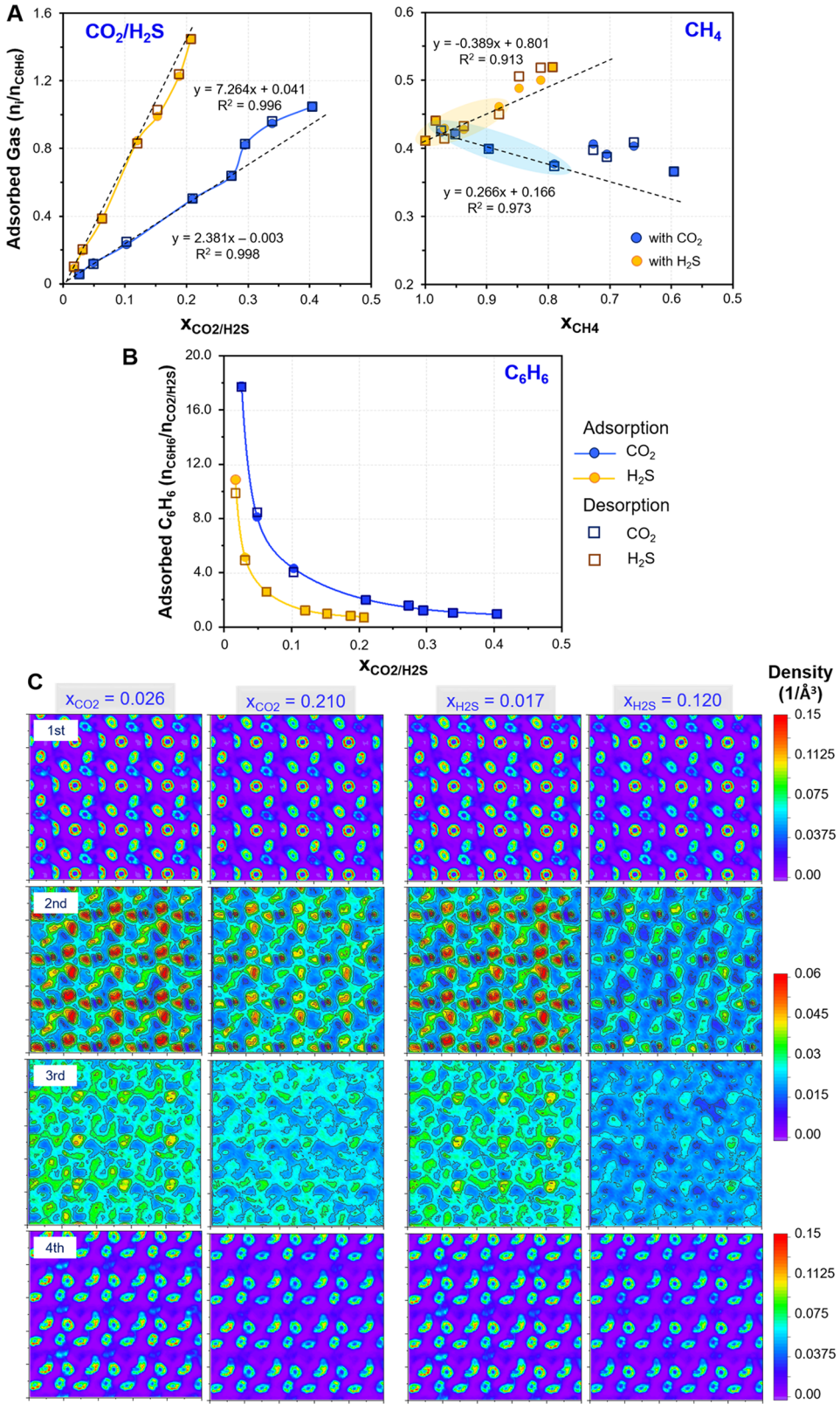

Figure 1. (A) Solubility of CO_2/H_2S (blue/yellow, left panel) and CH_4 (blue/yellow, right panel) inside the benzene-filled pore at 300 K as a function of CO_2/H_2S and CH_4 mole fractions, respectively, in the bulk reservoirs. (B) Amount of confined benzene per adsorbed CO_2/H_2S molecule as a function of CO_2 (blue) and H_2S (yellow) bulk mole fractions. Closed and open symbols represent data obtained during adsorption and desorption of CO_2/H_2S, respectively. (C) In-plane surface density distributions of benzene molecules within first, second, third, and fourth layers formed within the amorphous silica pore. Results are obtained for CO_2−CH_4 (left) and H_2S−CH_4 (right) mixtures at various CO_2/H_2S bulk mole fractions, as indicated above the panels. Details on computational procedures are available in the Supporting Information.

https://dx.doi.org/10.1021/acs.jpclett.9b03751
J. Phys. Chem. Lett. 2020, 11, 1814−1821

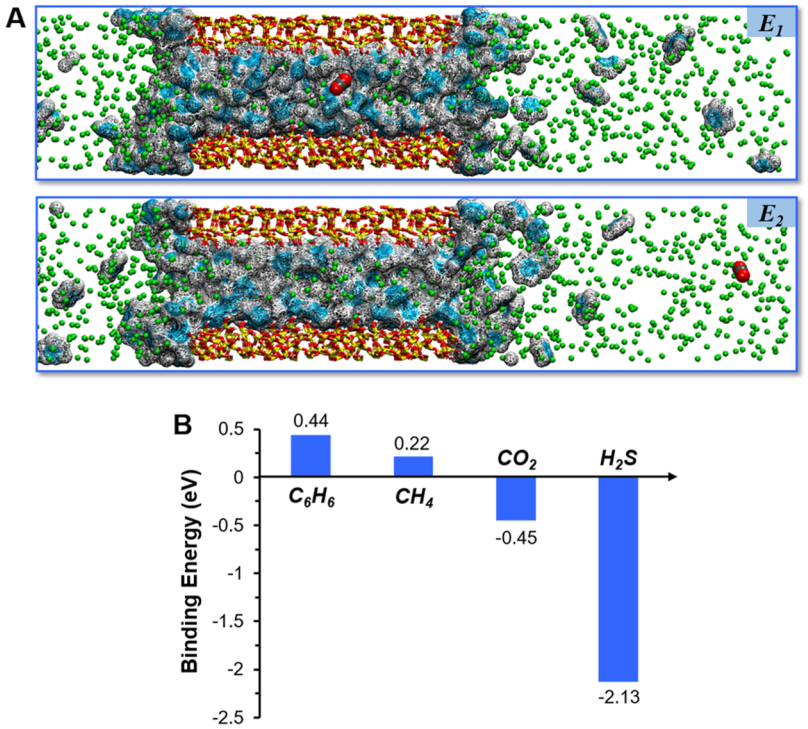

Figure 2. (A) Representative simulation snapshots for the calculation of average energies (one benzene, CH_4, CO_2, and H_2S molecule) within the SiO_2 pore filled with benzene and CH_4 (top) and in the bulk reservoirs containing only CH_4 (bottom) at 300 K. (B) Adsorption energies of benzene, CH_4, CO_2, and H_2S in the pore filled with benzene and CH_4.

The permeability of CO_2, H_2S, and CH_4 depends linearly on CO_2/H_2S bulk concentrations. Notably, the results show a decline in the rates of permeability increase for CH_4 mixed with CO_2 at CO_2 bulk mole fractions >0.05. The permeability of CH_4 mixed with H_2S is greater than that of CH_4 mixed with CO_2 at $x_{CO_2/H_2S} > 0.05$, indicating that ultilizing H_2S could be advantageous for improving shale gas extraction.

The transport diffusivity for the various gases can be extracted by dividing the permeability by the solubility within the nanopore.[36] We report solubility data for each species in Table S1. In interpeting those results, it should be noted that, as the bulk mole fraction of CH_4 decreases, the amount of benzene in the pore also decreases (see Figure 1B). We also computed the self-diffusivity for the various species inside the crowded pore using the Green−Kubo formulation.[37]

In Figure 3B, we present transport- (closed circles) and self- (open squares) diffusivity for CO_2 and H_2S (left panel, blue and yellow, respectively) and for CH_4 (right panel) for the various systems simulated. Similar to the permeability results, we observe a linear relation between transport (/self) diffusivities of CO_2/H_2S and the corresponding bulk mole fractions. However, the transport (/self) diffusivity of CH_4 first decreases upon loading CO_2/H_2S, and then increases. The results show that CH_4 diffuses faster than CO_2 and H_2S, achieving transport (/self) diffusivity of $\sim 2.4 \div 6.8 \times 10^{-9}$ m^2/s, as opposed to $\sim 2.25 \div 3.5 \times 10^{-9}$ m^2/s for CO_2 and H_2S when the CO_2 ($/H_2S$) mole fraction is <0.21 (/0.12). This is probably a consequence of the weaker attraction between CH_4 and the benzene-filled pore (see Figure 2). In contrast, although H_2S is more strongly adsorbed inside the pore than CO_2, it moves faster than CO_2, possibly because H_2S displaces more benzene from the pore than CO_2 does (see Figure 1B). At infinitely diluted conditions ($x_{CO_2/H_2S} \to 0$), the transport diffusivity of CO_2 and that of H_2S are similar ($\sim 2.3 \times 10^{-9}$ m^2/s). Recently, An et al.[38] conducted nuclear magnetic resonance experiments to measure methane diffusion in seven organic-rich shale samples from a Middle Eastern source rock. At ~13.9 MPa and ambient temperature, the methane diffusion coefficient was found to be $\sim 2 \div 6 \times 10^{-9}$ m^2/s, comparable to the results obtained here.

For isothermal mass transfer of pure species through a porous medium, transport diffusivity is generally greater than self-diffusivity, because interparticle correlations affect collective diffusivity, positively contributing to transport.[39] Our results differ from this general trend, because the transport diffusivity of all gases considered is slower than the corresponding self-diffusivity. This unexpected result is probably due to molecular clustering. Molecular clustering within pores is often ascribed to hydrogen bonding.[40] A recent experimental study provided evidence that the H_2S dimer has an anisotropic structure exhibiting one S−H···S hydrogen bond (HB).[41] In addition, the interactions between benzene and H_2S are due to SH-π interactions, a type of HB abundant in biological systems.[42] Preferential interactions between benzene and CO_2 (ref 30) could lead to clustering. Indeed, the surface density distributions for H_2S and CO_2 within various layers inside the crowded nanopore (Figure S8) provide conclusive proof of the existence of molecular clusters in our systems. These clusters appear to be more pronounced in the presence of H_2S rather than CO_2.

Although the value for the transport diffusivity of CO_2 ($/H_2S$) should approach the corresponding self-diffusivity, D_s, at low mole fraction, we observe a small deviation between D_t and D_s at $x_{CO_2/H_2S} \to 0$. This discrepancy is ascribed to uncertainties in the calculation of self-diffusivity using the Green−Kubo method, which is based on the integration of velocity−velocity autocorrelation functions over infinite times.[43]

https://dx.doi.org/10.1021/acs.jpclett.9b03751
J. Phys. Chem. Lett. 2020, 11, 1814−1821

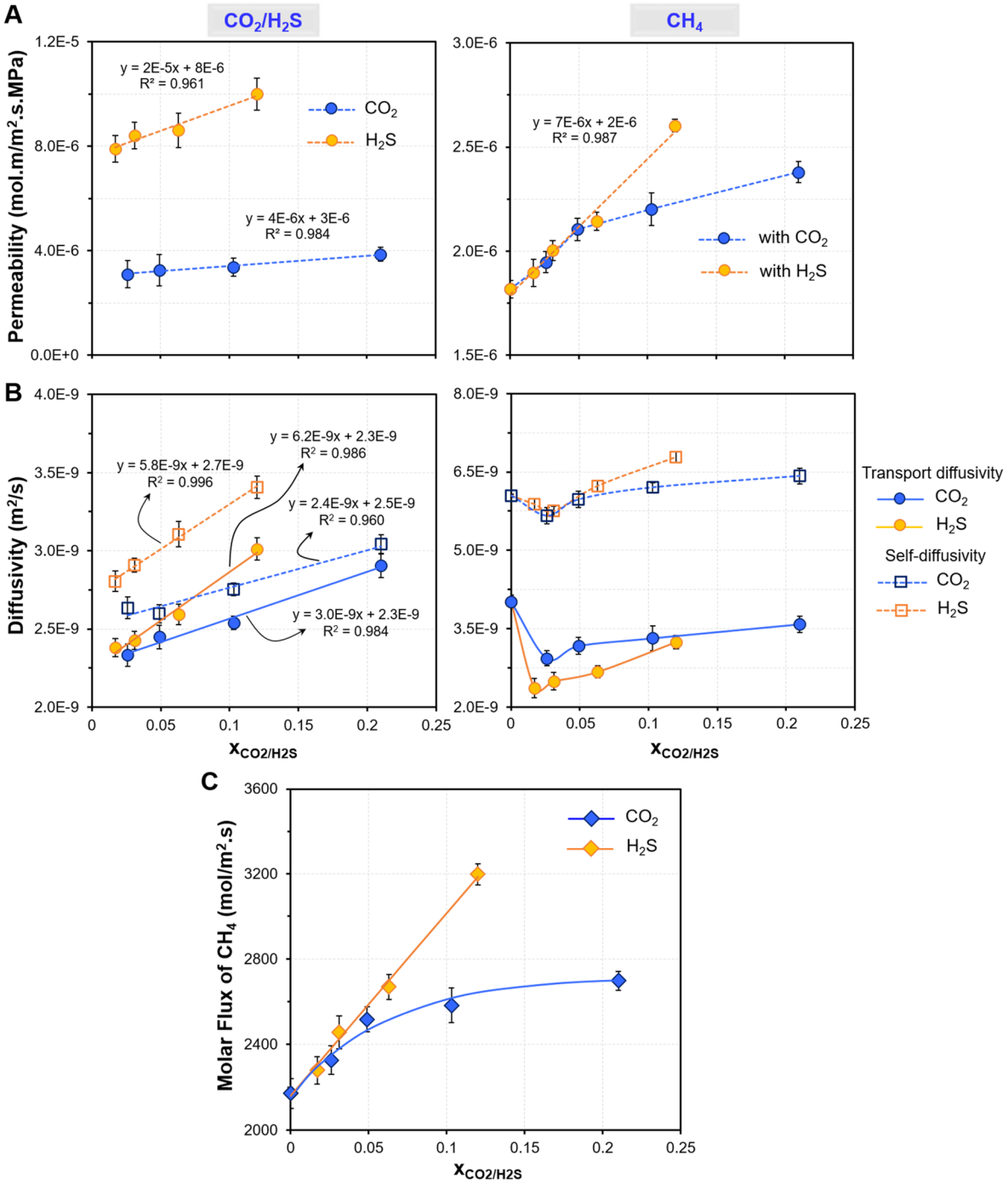

Figure 3. (A) Permeability and (B) transport diffusivity as determined by boundary driven nonequilibrium MD simulations across the benzene-filled pore for CO_2 and H_2S (blue and yellow closed symbols in the left panels, respectively) and CH_4 (right panels) for the various systems considered. Self-diffusivity data (open symbols), as determined by the Green−Kubo formulation, are also reported for CO_2/H_2S and CH_4 in panel B. (C) Molar flux of methane in CO_2−CH_4 (blue) and H_2S-CH_4 (yellow) mixtures across the benzene-filled SiO_2 nanopore as a function of CO_2/H_2S bulk mole fraction.

Although the transport diffusivity of CH_4 in the presence of either CO_2 or H_2S is slower than that for pure CH_4 (Figure 3B, right panel), we observe an increase of CH_4 molar flux when loading CO_2 or H_2S (Figure 3C). This confirms that CO_2 and H_2S play the role of carriers, facilitating CH_4 transport through the crowded nanopore.[44,45] The facilitated transport factors are estimated to be ∼1.46 and 1.77, respectively.

For solute transport through pores filled with solvents (i.e., our crowded SiO_2 pore), the local distribution of solvent molecules yields preferential transport pathways for the solute.[46,47] To better understand the transport behavior of CO_2, H_2S, and CH_4, we quantified free-energy (FE) landscapes by implementing well-tempered metadynamics.[48,49] The results for CO_2 and H_2S (panels A and B of Figure 4, respectively), show that the path connecting neighboring FE wells for CO_2 is longer and more tortuous than the one encountered by H_2S. However, to traverse the pore, H_2S molecules can jump only from one FE well to another, across barriers of ∼9 kcal/mol, whereas CO_2 encounters barriers of only ∼6.4 kcal/mol.[47] This suggests that the CO_2 molecule can travel more easily,

https://dx.doi.org/10.1021/acs.jpclett.9b03751
J. Phys. Chem. Lett. 2020, 11, 1814−1821

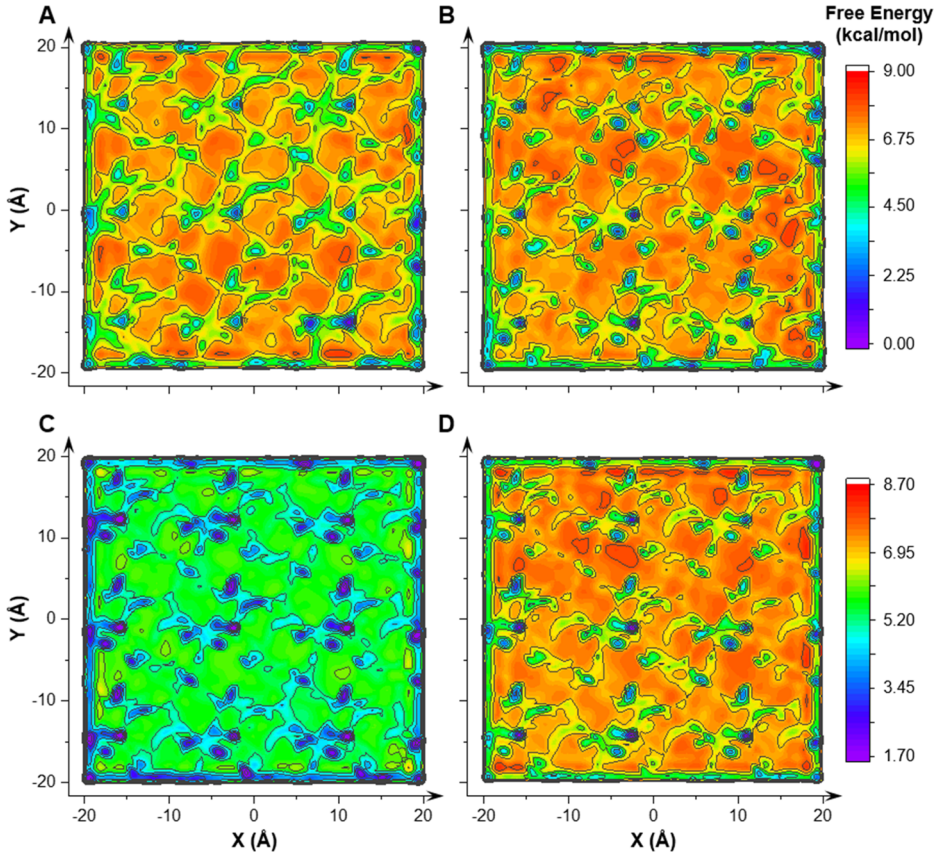

Figure 4. Free-energy landscapes projected onto planes parallel to the pore surface for one CO_2 (panel A) and one H_2S (panel B) molecule traveling inside the crowded nanopore (system 0, with composition shown in Table 1 and Figure S1), and that for one CH_4 molecule moving inside the pore of system 1C (panel C) and 1H (panel D). The results are obtained from well-tempered metadynamics simulations. The collective variables chosen are the components of the distance along the three Cartesian coordinates (x, y, z) between one molecule species i and the center of the benzene-filled pore.

notwithstanding the more tortuous path, compared to H_2S. In our systems, it appears that the longer path length that characterizes CO_2 transport is balanced by the lower FE barriers, as the pore diffusivity of CO_2 is similar to that for H_2S ($\sim 2.3 \times 10^{-9}$ m^2/s) at $x_{CO_2/H_2S} \to 0$.

In Figure 4C,D we found similar patterns connecting FE wells as experienced by CH_4 in systems 1C and 1H (in the presence of CO_2 and H_2S, respectively); however, in the presence of CO_2, deep FE wells appear, within which CH_4 molecules accumulate. Lower FE barriers are found in system 1C (~4.4 kcal/mol) compared to those observed for system 1H (~6.3 kcal/mol), likely due to the benzene−CO_2 interactions, which are weaker than those between benzene and H_2S. This difference in barriers seems to be correlated and potentially explains why the diffusivity of CH_4 in the pore of system 1C ($50CO_2$−1080 CH_4) is greater than that in system 1H ($50H_2S$−$1090CH_4$) (Figure 3B, right panel).

In conclusion, our simulations demonstrate that adding fluids such as CO_2 or H_2S impacts significantly fluid transport mechanisms in organic-rich sedimentary rocks. Particularly, CO_2/H_2S adsorption displaces and perhaps swells the organics, leading to noticeable differences for CH_4 solubility in confinement. More importantly, CO_2 and H_2S facilitate CH_4 transport through organic-rich caprock pores, acting as mobile carriers. Our results emphasize the importance of fluid−fluid and fluid−pore interactions, compounded by changes in the structure of confined fluids, in determining transport mechanisms of importance for geo-energy applications such as carbon sequestration in caprocks and enhanced hydrocarbon production and provide a general understanding of fluid transport in crowded pores frequently encountered in nature.

■ ASSOCIATED CONTENT

Supporting Information

The Supporting Information is available free of charge at https://pubs.acs.org/doi/10.1021/acs.jpclett.9b03751.

Details about simulation models, algorithms, implementation methods, calculation procedures and results for properties of interest such as density profiles, in-plane surface density distributions, adsorption isotherms, amount of benzene displaced, cross-sectional area, and solubility of all species (CO_2, H_2S, CH_4, and benzene) (PDF)

■ AUTHOR INFORMATION

Corresponding Authors

Anh Phan − *Department of Chemical Engineering, University College London, London WC1E 7JE, U.K.*; Email: anh.phan.13@ucl.ac.uk

Alberto Striolo − *Department of Chemical Engineering, University College London, London WC1E 7JE, U.K.*; orcid.org/0000-0001-6542-8065; Email: a.striolo@ucl.ac.uk

Complete contact information is available at: https://pubs.acs.org/10.1021/acs.jpclett.9b03751

https://dx.doi.org/10.1021/acs.jpclett.9b03751
J. Phys. Chem. Lett. 2020, 11, 1814−1821

Notes

The authors declare no competing financial interest.

■ ACKNOWLEDGMENTS

Generous allocations of computing time were provided by ARCHER, the UK National Supercomputing Service (http://www.archer.ac.uk) via our membership in the UK's HEC Materials Chemistry Consortium, which is funded by EPSRC (EP/L000202, EP/R029431), the University College London Research Computing Platforms Support (Myriad), the Oklahoma Supercomputing Center for Education and Research (OSCER), and the National Energy Research Scientific Computing Center (NERSC) at Lawrence Berkeley National Laboratory. NERSC is supported by the DOE Office of Science under Contract No. DE-AC02-05CH11231. This work is supported, in part by the Science4CleanEnergy European research consortium funded by European Union's Horizon 2020 research and innovation programme, under Grant Agreement No. 764810 (S4CE). The Authors are grateful to Dr Matteo Salvalaglio of University College London for interesting discussions during the preparation of the manuscript.

■ REFERENCES

(1) Bourg, I. C.; Beckingham, L. E.; DePaolo, D. J. The Nanoscale Basis of CO_2 Trapping for Geologic Storage. *Environ. Sci. Technol.* **2015**, *49*, 10265−10284.

(2) Mathias, S. A.; Gluyas, J. G.; Goldthorpe, W. H.; Mackay, E. J. Impact of Maximum Allowable Cost on CO_2 Storage Capacity in Saline Formations. *Environ. Sci. Technol.* **2015**, *49*, 13510−13518.

(3) Yang, C. B.; Trevino, R. H.; Zhang, T. W.; Romanak, K. D.; Wallace, K.; Lu, J. M.; Mickler, P. J.; Hovorka, S. D. Regional Assessment of CO_2-Solubility Trapping Potential: A Case Study of the Coastal and Offshore Texas Miocene Interval. *Environ. Sci. Technol.* **2014**, *48*, 8275−8282.

(4) IPCC. *IPCC Special Report on Carbon Dioxide Capture and Storage*; Cambridge University Press: Cambridge, U.K., 2005.

(5) Smit, B.; Reimer, J. R.; Oldenburg, C. M.; Bourg, I. C. *Introduction to Carbon Capture and Sequestration*; Imperial College Press: London, 2014.

(6) Bourg, I. C. Sealing Shales Versus Brittle Shales: A Sharp Threshold in the Material Properties and Energy Technology Uses of Fine-Grained Sedimentary Rocks. *Environ. Sci. Technol. Lett.* **2015**, *2*, 255−259.

(7) *Horn River Basin Unconventional Shale Gas Play Atlas*; BC Oil and Gas Commission; Fort Saint John, 2014.

(8) Weiland, R. H.; Hatcher, N. A. Overcome Challenges in Treating Shale Gases. *Hydrocarb Process* **2012**, *91*, 45−48.

(9) Cipolla, C. L.; Lolon, E. P.; Erdle, J. C.; Rubin, B. Reservoir Modeling in Shale-Gas Reservoirs. *Spe Reserv Eval Eng.* **2010**, *13*, 638−653.

(10) Tilley, B.; McLellan, S.; Hiebert, S.; Quartero, B.; Veilleux, B.; Muehlenbachs, K. Gas Isotope Reversals in Fractured Gas Reservoirs of the Western Canadian Foothills: Mature Shale Gases in Disguise. *AAPG Bull.* **2011**, *95*, 1399−1422.

(11) Parker, M.; Buller, D.; Petre, E.; Dreher, D. H. Haynesville Shale-Petrophysical Evaluation. In *SPE Rocky Mountain Petroleum Technology Conference*, Denver, CO, 2009; 122937.

(12) Pirzadeh, P.; Lesage, K. L.; Marriott, R. A. Hydraulic Fracturing Additives and the Delayed Onset of Hydrogen Sulfide in Shale Gas. *Energy Fuels* **2014**, *28*, 4993−5001.

(13) Maddox, R. N.; Morgan, J. Gas Treating and Sulfur Recovery. In *Gas Conditioning and Processing*; Campbell Petroleum Series: Norman, OK, 2006; Vol. 4.

(14) Snaebjornsdottir, S. O.; Oelkers, E. H.; Mesfin, K.; Aradottir, E. S.; Dideriksen, K.; Gunnarsson, I.; Gunnlaugsson, E.; Matter, J. M.; Stute, M.; Gislason, S. R. The Chemistry and Saturation States of Subsurface Fluids During the in Situ Mineralisation of CO_2 and H_2S at the Carbfix Site in Sw-Iceland. *Int. J. Greenhouse Gas Control* **2017**, *58*, 87−102.

(15) Hofmann, A.; van Strien, W.; Malekzadeh, R. Improving the Efficiency of H_2S Mitigation in Middle East Oil and Gas Fields. In *Abu Dhabi International Petroleum Exhibition & Conference*; Society of Petroleum Engineers: Abu Dhabi, UAE, 2017.

(16) Khan, C.; Amin, R.; Madden, G. Effects of CO_2 and Acid Gas Injection on Enhanced Gas Recovery and Storage. *J. Pet. Explor. Prod. Technol.* **2013**, *3*, 55−60.

(17) Falk, K.; Coasne, B.; Pellenq, R.; Ulm, F. J.; Bocquet, L. Subcontinuum Mass Transport of Condensed Hydrocarbons in Nanoporous Media. *Nat. Commun.* **2015**, *6*, 6949.

(18) Obliger, A.; Pellenq, R.; Ulm, F. J.; Coasne, B. Free Volume Theory of Hydrocarbon Mixture Transport in Nanoporous Materials. *J. Phys. Chem. Lett.* **2016**, *7*, 3712−3717.

(19) Apostolopoulou, M.; Dusterhoft, R.; Day, R.; Stamatakis, M.; Coppens, M.-O.; Striolo, A. Estimating Permeability in Shales and Other Heterogeneous Porous Media: Deterministic Vs. Stochastic Investigations. *Int. J. Coal Geol.* **2019**, *205*, 140−154.

(20) Phan, A.; Striolo, A. Methane Transport through Hierarchical Silica Micro-Mesoporous Materials: From Non-Equilibrium Atomistic Simulations to Phenomenological Correlations. *Microporous Mesoporous Mater.* **2019**, *288*, 109559.

(21) Rexer, T. F. T.; Benham, M. J.; Aplin, A. C.; Thomas, K. M. Methane Adsorption on Shale under Simulated Geological Temperature and Pressure Conditions. *Energy Fuels* **2013**, *27*, 3099−3109.

(22) Mosher, K.; He, J. J.; Liu, Y. Y.; Rupp, E.; Wilcox, J. Molecular Simulation of Methane Adsorption in Micro- and Mesoporous Carbons with Applications to Coal and Gas Shale Systems. *Int. J. Coal Geol.* **2013**, *109*, 36−44.

(23) Fischer, K.; Chen, J.; Petri, M.; Gmehling, J. Solubility of H_2S and CO_2 in N-Octyl-2-Pyrrolidone and of H_2S in Methanol and Benzene. *AIChE J.* **2002**, *48*, 887−893.

(24) Lay, E. N.; Taghikhani, V.; Ghotbi, C. Measurement and Correlation of CO_2 Solubility in the Systems of CO_2 Plus Toluene, CO_2 Plus Benzene, and CO_2 Plus N-Hexane at near-Critical and Supercritical Conditions. *J. Chem. Eng. Data* **2006**, *51*, 2197−2200.

(25) Phan, A.; Cole, D. R.; Striolo, A. Aqueous Methane in Slit-Shaped Silica Nanopores: High Solubility and Traces of Hydrates. *J. Phys. Chem. C* **2014**, *118*, 4860−4868.

(26) Ho, L. N.; Schuurman, Y.; Farrusseng, D.; Coasne, B. Solubility of Gases in Water Confined in Nanoporous Materials: Zsm-5, Mcm-41, and Mil-100. *J. Phys. Chem. C* **2015**, *119*, 21547−21554.

(27) Badmos, S. B.; Striolo, A.; Cole, D. R. Aqueous Hydrogen Sulfide in Slit-Shaped Silica Nanopores: Confinement Effects on Solubility, Structural, and Dynamical Properties. *J. Phys. Chem. C* **2018**, *122*, 14744−14755.

(28) Plimpton, S. Fast Parallel Algorithms for Short-Range Molecular-Dynamics. *J. Comput. Phys.* **1995**, *117*, 1−19.

(29) Heinz, H. Computational Screening of Biomolecular Adsorption and Self-Assembly on Nanoscale Surfaces. *J. Comput. Chem.* **2009**, *31*, 1564−1568.

(30) Chen, L.; Cao, F. L.; Sun, H. Ab Initio Study of the Pi-Pi Interactions between CO_2 and Benzene, Pyridine, and Pyrrole. *Int. J. Quantum Chem.* **2013**, *113*, 2261−2266.

(31) Ringer, A. L.; Figgs, M. S.; Sinnokrot, M. O.; Sherrill, C. D. Aliphatic C-H/Pi Interactions: Methane-Benzene, Methane-Phenol, and Methane-Indole Complexes. *J. Phys. Chem. A* **2006**, *110*, 10822−10828.

(32) Sinnokrot, M. O.; Sherrill, C. D. Highly Accurate Coupled Cluster Potential Energy Curves for the Benzene Dimer: Sandwich, T-Shaped, and Parallel-Displaced Configurations. *J. Phys. Chem. A* **2004**, *108*, 10200−10207.

(33) Sherrill, C. D.; Takatani, T.; Hohenstein, E. G. An Assessment of Theoretical Methods for Nonbonded Interactions: Comparison to Complete Basis Set Limit Coupled-Cluster Potential Energy Curves for the Benzene Dimer, the Methane Dimer, Benzene-Methane, and Benzene-H_2S. *J. Phys. Chem. A* **2009**, *113*, 10146−10159.

https://dx.doi.org/10.1021/acs.jpclett.9b03751
J. Phys. Chem. Lett. 2020, 11, 1814−1821

(34) Hill, R. J.; Jarvie, D. M.; Zumberge, J.; Henry, M.; Pollastro, R. M. Oil and Gas Geochemistry and Petroleum Systems of the Fort Worth Basin. *AAPG Bull.* **2007**, *91*, 445−473.
(35) Martini, A. M.; Walter, L. M.; McIntosh, J. C. Identification of Microbial and Thermogenic Gas Components from Upper Devonian Black Shale Cores, Illinois and Michigan Basins. *AAPG Bull.* **2008**, *92*, 327−339.
(36) Liu, J.; Jiang, J. W. Molecular Design of Microporous Polymer Membranes for the Upgrading of Natural Gas. *J. Phys. Chem. C* **2019**, *123*, 6607−6615.
(37) Dubbeldam, D.; Ford, D. C.; Ellis, D. E.; Snurr, R. Q. A New Perspective on the Order-N Algorithm for Computing Correlation Functions. *Mol. Simul.* **2009**, *35*, 1084−1097.
(38) An, Y.; Althaus, S. M.; Liu, H. H.; Chen, J. H. Nuclear Magnetic Resonance Measurement of Methane Diffusion in Organic-Rich Shales. *Fuel* **2019**, *247*, 160−163.
(39) Smit, B.; Maesen, T. L. M. Molecular Simulations of Zeolites: Adsorption, Diffusion, and Shape Selectivity. *Chem. Rev.* **2008**, *108*, 4125−4184.
(40) Krishna, R. Diffusion in Porous Crystalline Materials. *Chem. Soc. Rev.* **2012**, *41*, 3099−3118.
(41) Das, A.; Mandal, P. K.; Lovas, F. J.; Medcraft, C.; Walker, N. R.; Arunan, E. The H_2S Dimer Is Hydrogen-Bonded: Direct Confirmation from Microwave Spectroscopy. *Angew. Chem., Int. Ed.* **2018**, *57*, 15199−15203.
(42) Alberti, M.; Aguilar, A.; Huarte-Larranaga, F.; Lucas, J. M.; Pirani, F. Benzene-Hydrogen Bond (C_6H_6−HX) Interactions: The Influence of the X Nature on Their Strength and Anisotropy. *J. Phys. Chem. A* **2014**, *118*, 1651−1662.
(43) Oliveira, L. D.; Greaney, P. A. Method to Manage Integration Error in the Green−Kubo Method. *Phys. Rev. E: Stat. Phys., Plasmas, Fluids, Relat. Interdiscip. Top.* **2017**, *95*, 023308.
(44) Li, Y. F.; Wang, S. F.; He, G. W.; Wu, H.; Pan, F. S.; Jiang, Z. Y. Facilitated Transport of Small Molecules and Ions for Energy-Efficient Membranes. *Chem. Soc. Rev.* **2015**, *44*, 103−118.
(45) Wang, J. T.; Wang, S. F.; Xin, Q. P.; Li, Y. F. Perspectives on Water-Facilitated CO_2 Capture Materials. *J. Mater. Chem. A* **2017**, *5*, 6794−6816.
(46) Phan, A.; Cole, D. R.; Weiss, R. G.; Dzubiella, J.; Striolo, A. Confined Water Determines Transport Properties of Guest Molecules in Narrow Pores. *ACS Nano* **2016**, *10*, 7646−7656.
(47) Bui, T.; Phan, A.; Cole, D. R.; Striolo, A. Transport Mechanism of Guest Methane in Water-Filled Nanopores. *J. Phys. Chem. C* **2017**, *121*, 15675−15686.
(48) Barducci, A.; Bussi, G.; Parrinello, M. Well-Tempered Metadynamics: A Smoothly Converging and Tunable Free-Energy Method. *Phys. Rev. Lett.* **2008**, *100*, 020603.
(49) Bonomi, M.; Branduardi, D.; Bussi, G.; Camilloni, C.; Provasi, D.; Raiteri, P.; Donadio, D.; Marinelli, F.; Pietrucci, F.; Broglia, R. A.; Parrinello, M. Plumed: A Portable Plugin for Free-Energy Calculations with Molecular Dynamics. *Comput. Phys. Commun.* **2009**, *180*, 1961−1972.

https://dx.doi.org/10.1021/acs.jpclett.9b03751
J. Phys. Chem. Lett. 2020, 11, 1814−1821